Supporting Information

The Influence of Electrostatics on Small Molecule Flux through a Protein Nanoreactor

Jeff E. Glasgow, Michael A. Asensio, Christopher M. Jakobson, Matthew B. Francis, and Danielle Tullman-Ercek

Kinetic Modeling

Species

S^* substrate in assay solution (constant)

S substrate inside capsid

I inhibitor inside capsid

P product total (observable)

Rates

$$\frac{dS^*}{dt} = 0$$

$$\frac{dS}{dt} = -\frac{1}{F_V}\frac{dP}{dt} + k_1(S^* - S)$$

$$\frac{dI}{dt} = \frac{1}{F_V}\frac{dP}{dt} - k_2 I$$

$$\frac{dP}{dt} = \frac{k_{cat}S}{K_M\left(1 + \frac{I}{K_I}\right) + S}$$

Parameters

k_1 substrate transport

k_2 inhibitor transport

k_{cat} catalytic rate constant

K_M Michaelis-Menten constant

K_I competitive inhibition constant

F_V volume fraction of assay solution that is capsid lumen (~10^{-7})

Key assumptions

Michaelis-Menten kinetics with competitive product inhibition by phosphate

$\frac{dS^*}{dt} = 0$ (very large reservoir of substrate in the assay bulk)

$I = 0$ outside capsid (assay bulk is very large relative to capsid phase)

Intrinsic k_{cat}, K_M of enzymes unchanged by encapsulation in $MS2^{T71E}$ relative to $MS2^{WT}$

Rate of formation of product is normalized to enzyme concentration for comparison with experiment

Calculation of apparent diffusivities from fitted parameters

Consider the diffusive flux of substrate S as modeled: $J_M = k_2(S^* - S)[=]\frac{mol}{L-s}$, as compared to the diffusive flux $J_F = D_2\frac{(S^*-S)}{L}[=]\frac{mol}{m^2-s}$, where D_2 is the apparent diffusivity and L is the characteristic length of the flux.

We desire D_2 in terms of the fitted parameter k_2.

First, convert both fluxes to absolute flux in $\frac{mol}{s}$.

$$J_{abs} = J_F * A_{capsid} = \left(D_2\frac{(S^* - S)}{L}\right)A_{capsid}$$

$$J_{abs} = J_M * V_{capsid} = \left(k_2(S^* - S)\right)V_{capsid}$$

$$A_{capsid} = 4\pi\varepsilon R^2$$

Where ε is the fraction of the capsid surface area occupied by the pores. Considering that the diffusing molecule has a hydrodynamic diameter of ~6 Å and the pore has a diameter of ~18 Å, we consider the pore as having a radius as follows: $R_{pore} = \frac{18-6}{2} = 6$ Å.

$$\varepsilon = \frac{32 * \pi {R_{pore}}^2}{4\pi R^2} = 0.016$$

$$V_{capsid} = \frac{4}{3}\pi R^3$$

$$\therefore J_{abs} = \left(D_2\frac{(S^* - S)}{L}\right)4\pi\varepsilon R^2 = \left(k_2(S^* - S)\right)\frac{4}{3}\pi R^3$$

$$\left(\frac{D_2}{L}\right) = (k_2)\frac{1}{3}\frac{R}{\varepsilon}$$

$$D_2 = \frac{1}{3}\frac{RLk_2}{\varepsilon}$$

The characteristic length L is approximately the thickness of the capsid shell (1 nm) and the radius of the capsid R is approximately 13 nm.

Typically, D_2 has units of $\frac{cm^2}{s}$ and in this case k_2 has units of $\frac{1}{s}$. Thus, we can find D_2 as follows.

$$D_2 = \frac{1}{3}\frac{RLk_2}{\varepsilon} = 1.64x10^{-9}\frac{cm^2}{s}$$

For comparison, the diffusivity of phosphate in water at infinite dilution at 25ºC is $D_\infty \approx 5x10^{-6}\frac{cm^2}{s}$ and the diffusivity of atomic carbon in iron at 25ºC is $D \approx 10^{-12}\frac{cm^2}{s}$. We attribute this dramatic decrease in apparent diffusivity to the fact that the Debye length of the system is on the same order of magnitude as the pore radius, indicating that the electrical double layer likely penetrates far into the pore. There is thus a strong electrostatic repulsion between the negatively charged amino acid residues in the vicinity of the pore and the negatively charged substrate and phosphate species, greatly hindering diffusion through the capsid pore. This repulsion is modulated by the amino acid character of the pore residues, as evidenced by the differences in kinetic behavior between the $MS2^{WT}$ and $MS2^{T71E}$ capsid systems.

Smith and Deen[1] develop a theory for a system of charged spheres diffusing in charged pores similar to our system, and find that the Boltzmann factor $\frac{-E(r)}{kT}$ (where $\frac{D}{D_\infty} \propto \int exp\left[\frac{-E(r)}{kT}\right] rdr$) becomes vanishingly small as the ratio of pore size to Debye length approaches 2, as is the case for our system. Although they considered somewhat larger pores (~10 nm), their findings are in agreement with our observations.

Supplementary Figures and Tables

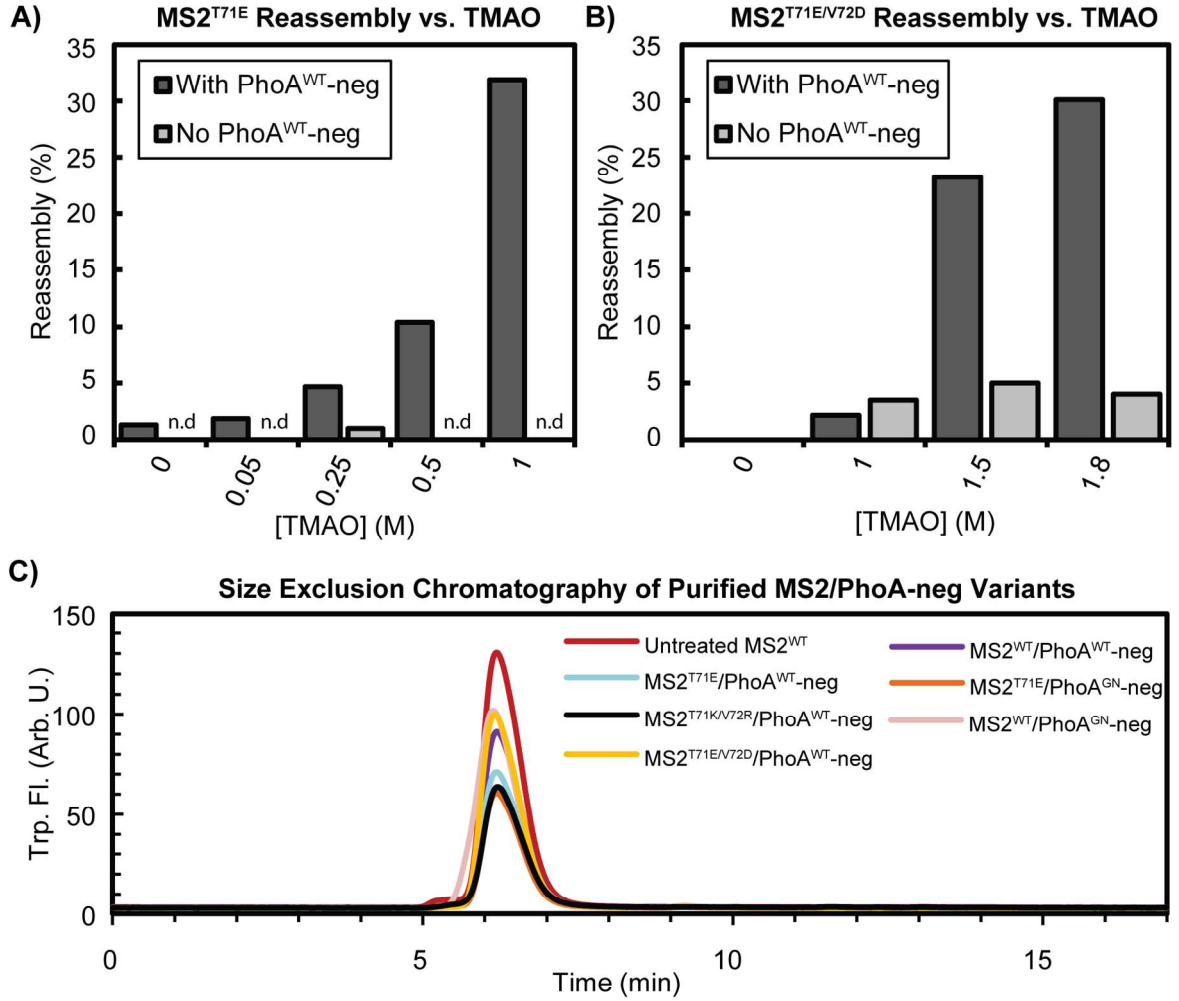

Supplemental Figure S1. Reassembly of capsid mutants around PhoA^{WT}-neg. A) MS2^{T71E} reassembly around PhoA^{WT}-neg in Bis Tris pH 6.0 is greatly enhanced by high concentrations of trimethylamine-*N*-oxide (TMAO). B) MS2$^{T71E/V72D}$ reassembly is also enhanced by TMAO. No significant reassembly was observed below 1 M. Background reassembly, though minimal, may result in some empty capsids. C) Size exclusion chromatography of all purified enzyme/capsid combinations. All have the same retention time and show no detectable free enzyme, even after 2 months of storage at 4 ^{o}C.

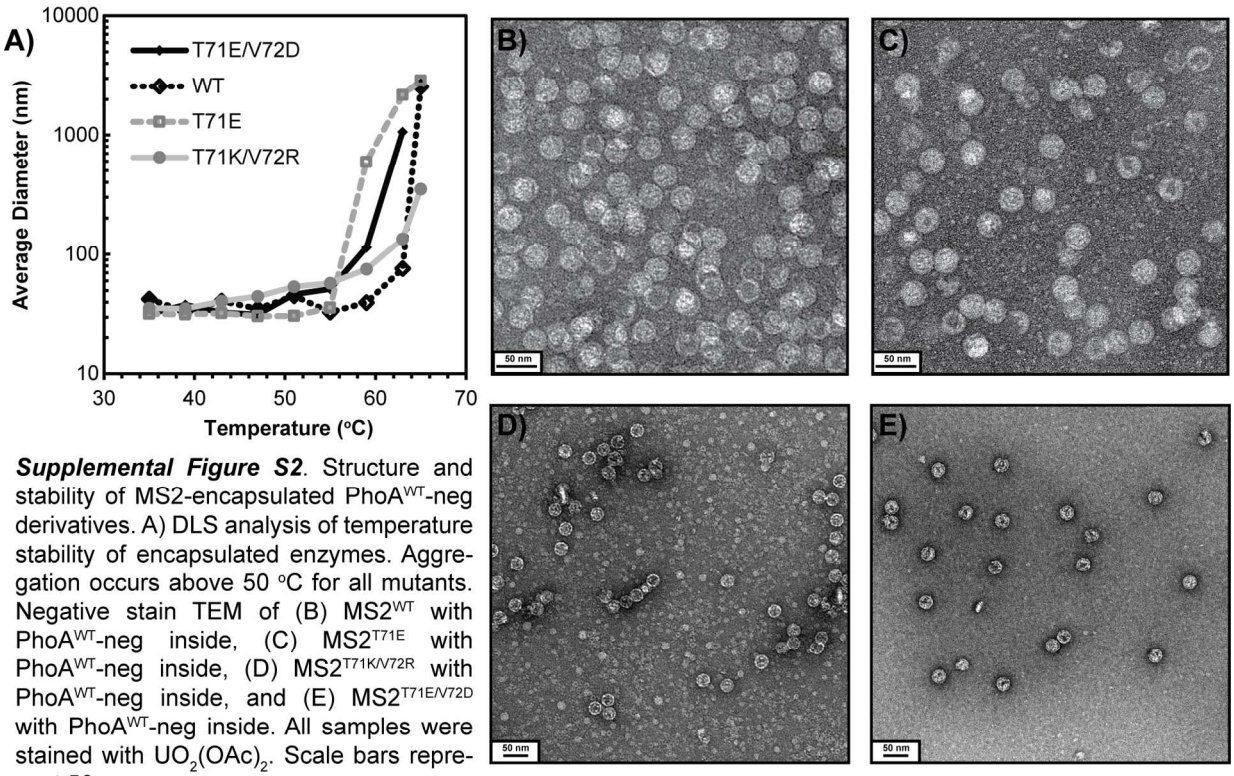

Supplemental Figure S2. Structure and stability of MS2-encapsulated PhoA^{WT}-neg derivatives. A) DLS analysis of temperature stability of encapsulated enzymes. Aggregation occurs above 50 °C for all mutants. Negative stain TEM of (B) MS2^{WT} with PhoA^{WT}-neg inside, (C) MS2^{T71E} with PhoA^{WT}-neg inside, (D) MS2$^{T71K/V72R}$ with PhoA^{WT}-neg inside, and (E) MS2$^{T71E/V72D}$ with PhoA^{WT}-neg inside. All samples were stained with $UO_2(OAc)_2$. Scale bars represent 50 nm.

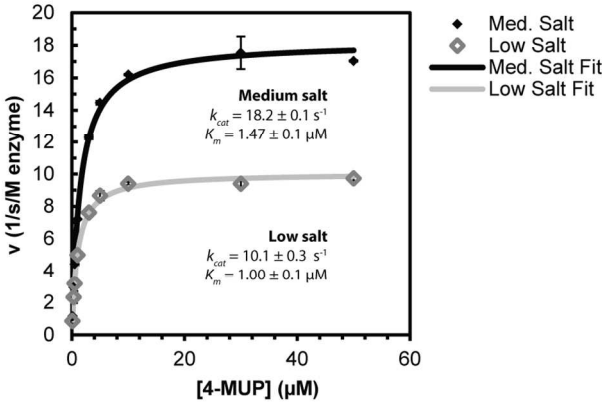

Supplemental Figure S3. Kinetics of free PhoA^{WT}-neg in medium and low salt Tris buffer after treatment with reassembly and purification conditions. Slight changes were observed in the kinetic parameters k_{cat} and K_M, but do not account for changes observed in encapsulated derivatives.

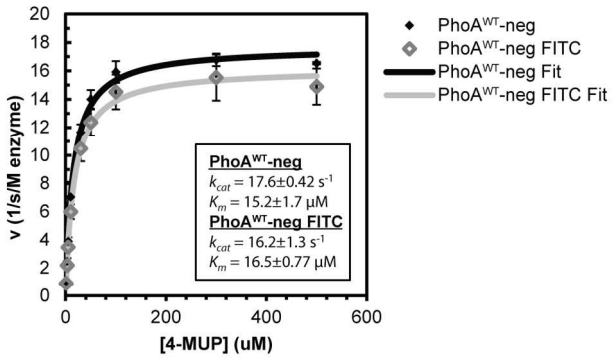

Supplemental Figure S4. Analysis of kinetics of FITC-labeled and unlabeled PhoA^{AW}T-neg in high salt MOPS.

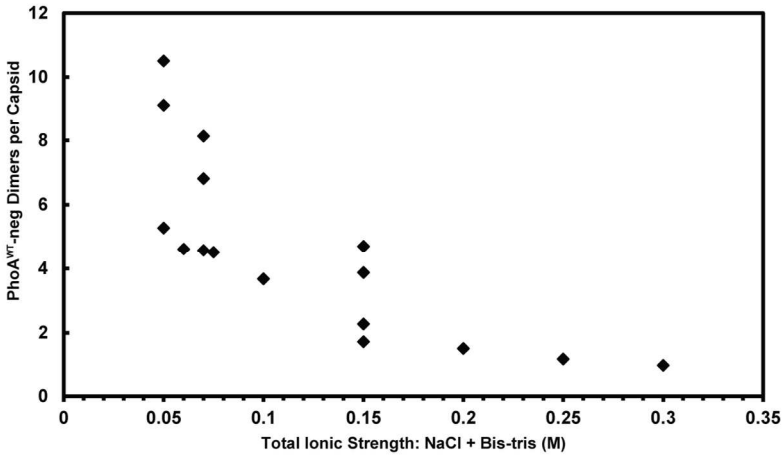

Supplemental Figure S5. Loading of PhoA^{WT}-neg in MS2^{WT} varies inversely with ionic strength of the reassembly reaction. NaCl was added to increase the ionic strength; 0.05 M Bis-tris was present in all reassembly conditions. Each data point represents a separate reassembly reaction. Error of enzyme quantification is not shown.

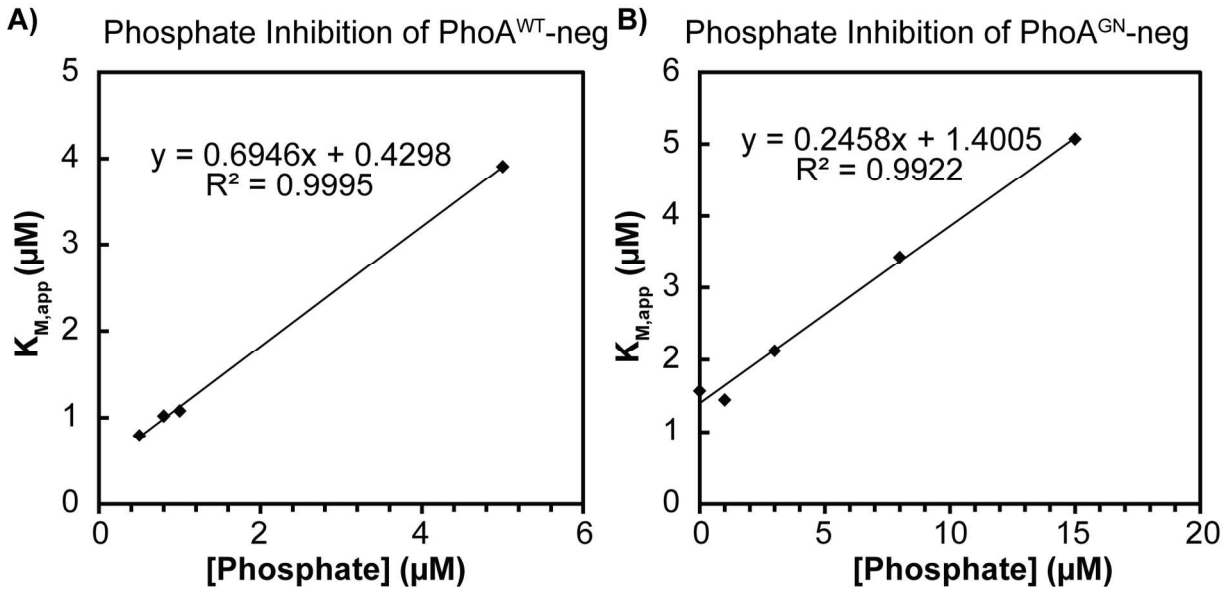

Supplemental Figure S6. Experimental determination of K_i for A) Free PhoA^{WT}-neg and B) PhoA$^{D153G/D330N}$-neg in medium salt Tris buffer.

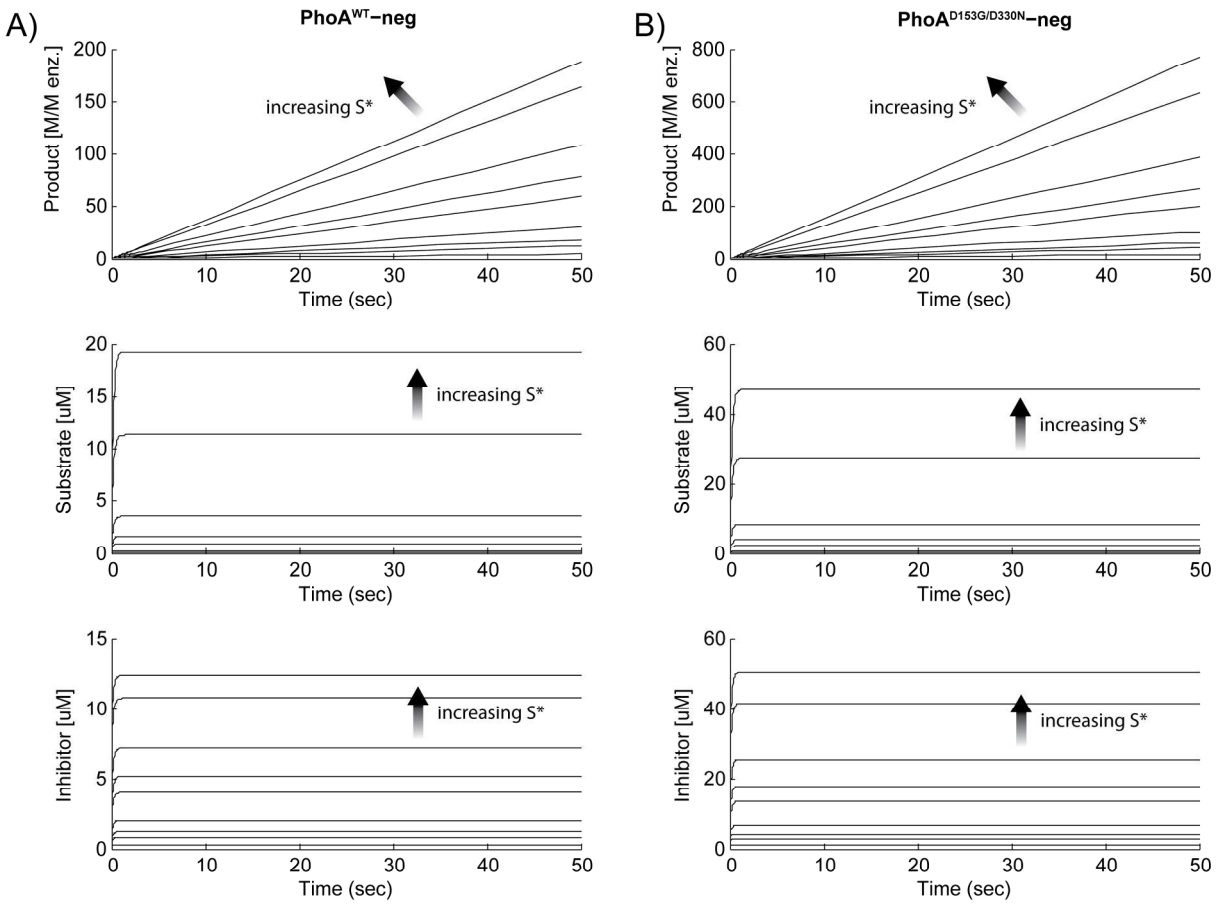

Supplemental Figure S7. Simulated concentration profiles for the product, substrate, and competitive inhibitor are shown for each experimental substrate concentration for the A.) PhoA^{WT}-neg and B.) PhoA$^{D153G/D330N}$-neg cases. Product concentration is shown for the assay bulk and capsid phases combined, as observed by experiment; substrate and inhibitor concentrations are the intra-capsid concentrations. A linear regression was performed to determine the initial rate of product formation at each substrate concentration. Substrate and inhibitor concentrations were both observed to reach a pseudo-steady state over the timescale of the simulation.

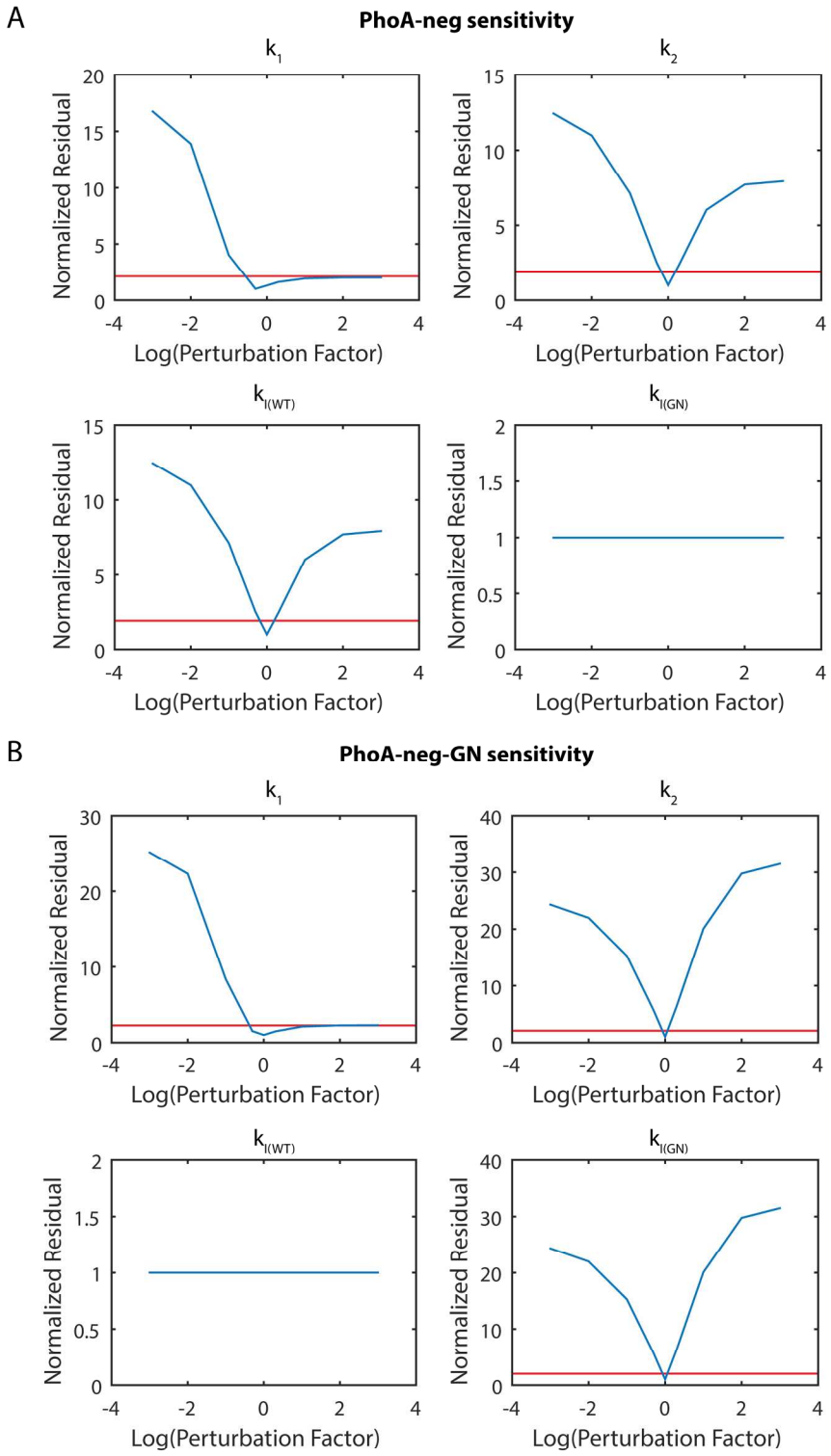

Supplemental Figure S8. Sensitivity analysis for kinetics parameters. The residual (sum of the square errors) of T71E MS2 capsid kinetics model relative to the experimental data is shown for A.) PhoA-neg and B.) PhoA-neg-GN with each fitted kinetic parameter (k_1, k_2, KI_{wt}, and KI_{GN}) multiplied by the perturbation factor (ranging from 0.001 to 1000). The residuals are normalized to the best fit found by the nonlinear minimization routine. The red line on each plot indicates a normalized residual of 2. The goodness of fit of the model is found not to be sensitive to increases in the substrate diffusion parameter k_1, but is found to be sensitive to decreases in the substrate diffusion parameter k_1, and to the phosphate diffusion parameter k_2 and the competitive inhibition parameters KI_{wt} and KI_{GN}.

Mutant	Primer
T71E	5'-GGTGCCTAAAGTGGCAACCCAGGAGGTTGGTGGTGTAGAGC-3'
	5'-GCTCTACACCACCAACCTCCTGGGTTGCCACTTTAGGCACC-3'
T71E/V72D	5'-GGTGCCTAAAGTGGCAACCCAGGAGGACGGTGGTGTAGAGC-3'
	5'-GCTCTACACCACCGTCCTCCTGGGTTGCCACTTTAGGCACC-3'
T71K/V72R	5'-GGTGCCTAAAGTGGCAACCCAGAAACGCGGTGGTGTAGAGC-3'
	5'-GCTCTACACCACCGCGTTTCTGGGTTGCCACTTTAGGCACC-3'

Supplementary Table S1. Mutagenesis primers for MS2 capsid pore mutants.

Capsid and Enzyme Type	**Average Enzyme Dimers/Capsid**
WT/PhoA-neg	9.6
T71E/PhoA-neg	5.8
T71E/V72D/PhoA-neg	3
T71K/V72R/PhoA-neg	9.4
WT/PhoA$^{D153G/D330N}$-neg	9.5
T71E/ PhoA$^{D153G/D330N}$-neg	6

Supplementary Table S2. Enzyme loading in MS2 derivatives. Enzyme concentration was measured by SDS-PAGE densitometry. Total protein was measured by A_{280} using $\varepsilon = 0.71$ cm·mL/mg for PhoA-neg and $\varepsilon = 1$ cm·mL/mg for MS2.

		Free	WT	E	ED	KR
Tris High Salt	k_{cat} (s^{-1})	23.8 ± 3.8	13.21 ± 1.0	19.7 ± 1.6	16.9 ± 2.0	18.3 ± 2.46
	$K_{M,app}$ (μM)	2.13 ± 0.09	2.59 ± 0.30	13.4 ± 0.24	5.72 ± 0.22	2.76 ± 0.12
Tris Medium Salt	k_{cat} (s^{-1})	11.6 ± 0.83	5.40 ± 0.34	4.75 ± 0.57	4.87 ± 1.0	8.79 ± 1.1
	$K_{M,app}$ (μM)	0.97 ± 0.02	1.0 ± 0.02	4.8 ± 0.63	2.18 ± 0.29	1.0 ± 0.07
Tris Low Salt	k_{cat} (s^{-1})	5.23 ± 0.25	2.51 ± 0.12	2.74 ± 0.30	2.59 ± 0.30	4.68 ± 0.57
	$K_{M,app}$ (μM)	0.54 ±0.003	0.89 ± 0.03	2.13 ± 0.15	1.89 ± 0.16	0.56 ± 0.03
MOPS Low Salt	k_{cat} (s^{-1})	7.58 ± 0.02	4.89 ± 0.33	4.40 ± 0.34	4.06 ± 0.57	n.d.
	$K_{M,app}$ (μM)	2.31 ± 0.07	3.79 ± 0.29	6.87 ± 0.71	6.42 ± 0.50	n.d.
Tris Medium Salt ($PhoA^{D153G/D330N}$ mutant)	k_{cat} (s^{-1})	43.3 ± 8.1	31.4 ± 5.3	19.8 ± 5.3	n.d.	n.d.
	$K_{M,app}$ (μM)	1.43 ± 0.16	2.45 ± 0.10	15.0 ± 1.8	n.d.	n.d.

Supplementary Table S3. Kinetic constants for free and encapsulated PhoA-neg and $PhoA^{D153G/D330N}$-neg derivatives in several conditions all show substantial increases in $K_{M,app}$. Error represents aggregation of standard deviations from at least three kinetic assays using nine substrate concentrations and at least three SDS-PAGE densitometry measurements to determine enzyme concentration.

References

(1) Smith III, F. G., and Deen, W. M. (1980) Electrostatic double-layer interactions for spherical colloids in cylindrical pores. *J. Colloid Interface Sci. 78*, 444–465.